communications biology

A Nature Portfolio journal

Article

https://doi.org/10.1038/s42003-025-09093-6

CCDC141 is a Connectin/Titin and Nesprin-1 binding protein that adapts cardiomyocytes to mechanical stress

Akira Hanashima[1] ✉, Misaki Kimoto[1], Yoshihiro Ujihara[2], Ken Hashimoto[1], Yuu Usui[3], Momoko Ohira[1], Masato Hoshino[4], Kentaro Uesugi[4], Stephanie Witt[5], Dittmar Labeit[6], Sumiko Kimura[7], Takashi Murayama[8], Takashi Sakurai[8], Siegfried Labeit[6] & Satoshi Mohri[1]

The heart adapts to mechanical stresses such as hypertension, yet the underlying mechanisms remain poorly understood. We identify CCDC141 as a mechanoadaptive factor in cardiomyocytes. CCDC141 interacts with the sarcomeric connectin/titin filament system and the nuclear envelope protein nesprin-1, and localizes to the costameres in adult cardiomyocytes. CCDC141-KO mouse cardiomyocytes exhibit hypertrophy. Their mitochondria display abnormal alignment and fusion, are burdened by elevated ATP production, and show reduced spare respiratory capacity. Increased SERCA2a expression enhances Ca^{2+} handling within the sarcoplasmic reticulum of CCDC141-KO cardiomyocytes. During pressure overload-induced heart failure in mice, CCDC141 relocalizes to the nuclear envelope, suggesting a stress-responsive role in maintaining nuclear integrity. CCDC141-KO hearts show low tolerance to mechanical stress, and despite only moderate pressure overload induced by transverse aortic constriction, they are more susceptible to fatal arrhythmias and progressive heart failure with disrupted nuclear morphology. These findings provide new insights into the molecular basis of cardiac mechanoadaptation and disease.

The heart adapts to mechanical overloads, such as hypertension, through myocardial hypertrophy. However, long-term hypertrophy may lead to heart failure. During this process, cardiomyocytes sense mechanical stress and alter their structural functions through signal transduction. Intracellular tension-transducing networks, including connectin/titin, nesprins, and costameres, act as mechanosensors in cardiomyocytes, along with the channels and receptors on the plasma membrane[1].

Connectin, also called titin, is a giant myoelastic protein (approximately 3000 kDa) that connects the thick filaments to the Z-lines of the cardiomyocyte sarcomeres, generating passive tension during relaxation to modulate cardiac dilatability[2]. Its I-band region functions as a molecular spring, adapting to developmental mechanical changes by switching from the compliant N2BA isoform to the stiffer N2B isoform[3]. The N2B and N2A segments bind to various signaling molecules to initiate mechanotransduction[4]. Meanwhile, the A-band region binds to the myosin filaments. Within its P-zone, which contains a kinase domain, connectin binds to the muscle-specific RING finger-1 and 2 (MuRF1, MuRF2) E3 ubiquitin ligases, regulating proteolysis in response to mechanical tension[5].

Nesprins bind to the SUN (Sad1p and UNC-84 homology) proteins at the nuclear envelope to form the LINC (linker of nucleoskeleton and cytoskeleton) complex, which transduces extracellular mechanical stimuli to the nucleus[6] and alters gene expression to adapt to mechanical loading. Double knockout of nesprin-1,2 causes premature cardiomyopathy[7], while deletion of the nesprin-1 KASH (Klarsicht/Anc-1/SYNE homology) domain develops cardiomyopathy with cardiac stimulatory conduction system disease[8].

Costameres interconnect the cell adhesion molecule integrin to the sarcomere Z-line, which transmits mechanical stress outside the cardiomyocyte to the Z-line and the sarcomere-generated forces to the adjacent myocytes. Through mechanotransduction, integrins modulate cardiac hypertrophy, contractility, and Ca^{2+} handling under physiological

[1]First Department of Physiology, Kawasaki Medical School, Kurashiki, Japan. [2]Department of Electrical and Mechanical Engineering, Graduate School of Engineering, Nagoya Institute of Technology, Nagoya, Japan. [3]Division of Biomechanics and Signaling, Institute of Advanced Medical Sciences, Tokushima University, Tokushima, Japan. [4]Japan Synchrotron Radiation Research Institute (SPring-8), Hyogo, Japan. [5]Department of Genetic Epidemiology in Psychiatry, Central Institute of Mental Health, Medical Faculty Mannheim, Heidelberg University, Mannheim, Germany. [6]DZHK Partnersite Mannheim-Heidelberg, Department of Integrative Pathophysiology, Medical Faculty Mannheim, Heidelberg University, Mannheim, Germany. [7]Department of Biology, Faculty of Science, Chiba University, Chiba, Japan. [8]Department of Pharmacology, Juntendo University School of Medicine, Tokyo, Japan. ✉e-mail: hanashima@med.kawasaki-m.ac.jp

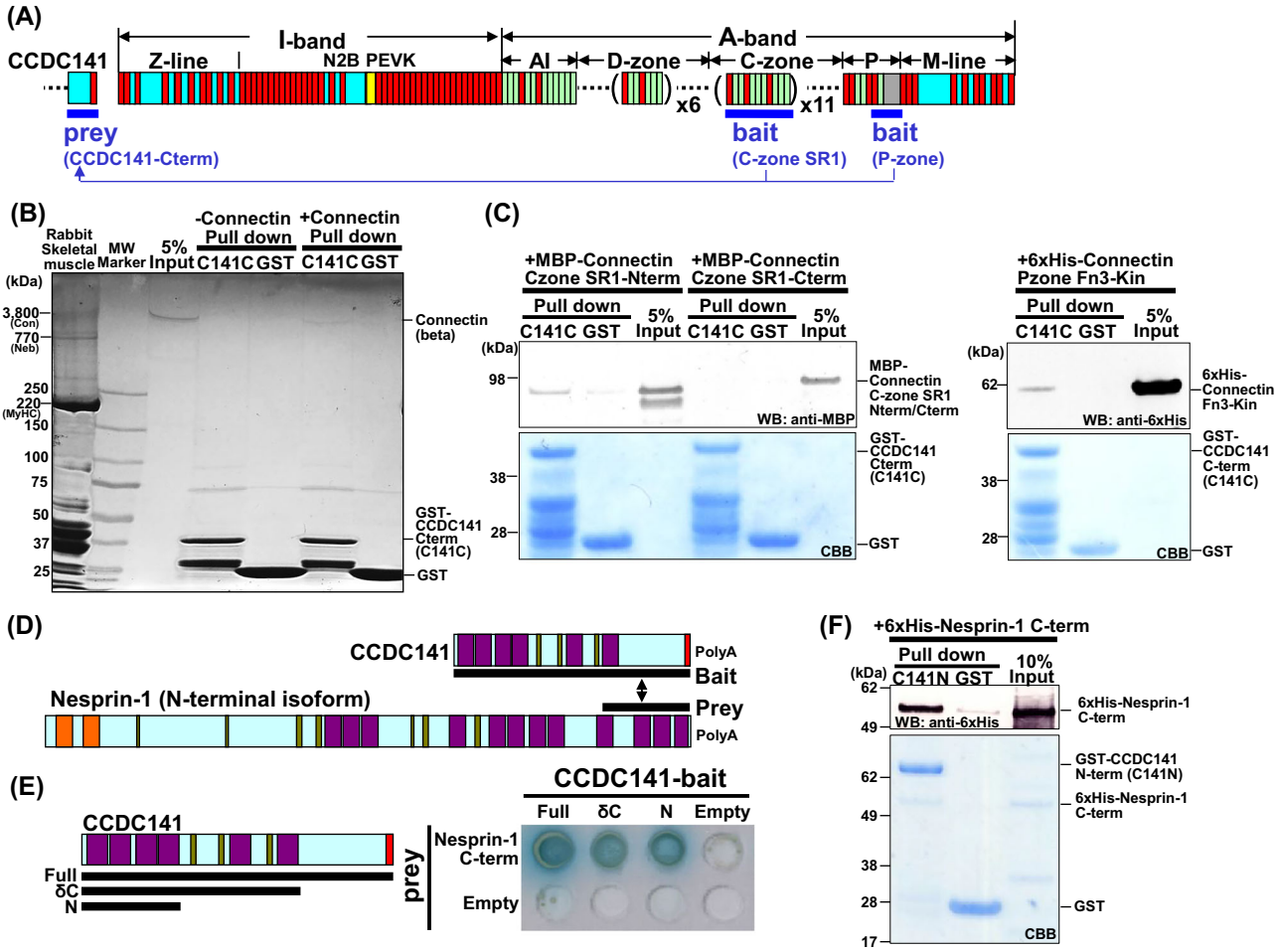

Fig. 1 | CCDC141 is a novel connectin/titin and nesprin-1 binding protein. **A** Yeast two-hybrid screening of binding proteins on the connectin A-band. CCDC141 binds to the connectin C-zone or P-zone and is transcribed from a gene adjacent to the connectin gene. Red box, Ig domain. Yellow box, PEVK segment. Light green box, Fn3 domain. Gray box, Kinase domain. Light blue box, Unique sequence. **B** Pull-down experiments of CCDC141 C-terminus (GST-tag) with isolated β-connectin/ titin-II. **C** Pull-down experiments of CCDC141 C-terminus (GST-tag) with the C-zone super-repeat 1 N-terminus (MBP-tag), C-zone super-repeat 1 C-terminus (MBP-tag), or P-zone Fn3-Kinase fragment (6×His-tag) of connectin. CBB, Coomassie brilliant blue. **D** Yeast two-hybrid screenings of CCDC141 binding proteins. Nesprin-1 was identified as a CCDC141 binding protein. Orange box, Calponin homology domain. Purple box, Spectrin repeat. Olive green box, Coiled-coil motif. Red box, Ig domain. **E** Yeast two-hybrid assay using truncated CCDC141 and screened nesprin-1 fragments. The N-terminal spectrin repeats of CCDC141 bound to the spectrin repeats of nesprin-1. **F** Pull-down experiment using GST-tagged CCDC141 N-terminus and 6xHis-tagged nesprin-1. Bound nesprin-1 was detected by western blot using anti-polyhistidine antibody (upper panel) and Coomassie brilliant blue staining (lower panel).

conditions. In response to mechanical cues, costameres and Z-lines recruit PI3K-regulated binding molecules to maintain cardiomyocyte homeostasis[9].

The *CCDC141* gene is connected upstream of the connectin gene[10]. Genome-wide association studies showed that CCDC141 was associated with heart rate[11], QT interval[12], QRS duration[13], QRS complex of the ECG[14], blood pressure[15,16], cardiac hypertrophy[17], supraventricular arrhythmias[18], and bradyarrhythmia development[19]. These associations suggest that CCDC141 may serve as a potential therapeutic target for improving cardiac function. However, its role in the heart remains uncharacterized.

In this study, we show that CCDC141 is a novel connectin and nesprin-1 binding protein that localizes to costameres in adult cardiomyocytes and to the nuclear envelope during mechanical overload-induced heart failure. We further show that CCDC141-KO hearts exhibit impaired adaptive capacity to mechanical stress through alterations in mitochondrial metabolism and cardiomyocyte Ca^{2+} handling.

Results

CCDC141 is a novel connectin and nesprin-1 binding protein

The connectin A-band region is a force-generating site for actin-myosin interactions, but its mechanotransduction is not well understood. We screened the binding proteins of the connectin A-band region using the yeast two-hybrid method (Fig. 1A). Pull-down experiments confirmed that the CCDC141 C-terminus can bind to isolated β-connectin/titin-2, including the connectin A-band region (Fig. 1B), as well as to the C-zone and P-zones of the connectin A-band region (Fig. 1C). Next, we screened CCDC141 binding proteins and confirmed that its N-terminal spectrin repeats can bind to the nesprin-1 spectrin repeats using the yeast two-hybrid assays (Fig. 1D, E) and pull-down experiments (Fig. 1F). These results indicate that CCDC141 is a novel connectin- and nesprin-1-binding protein.

CCDC141 is highly expressed in cardiomyocytes

CCDC141 gene is located adjacent to the connectin gene (*Ttn*) and shares an overlapping transcriptional unit (Fig. 2A). The human CCDC141 gene spans 220 kb and comprises 24 exons. Multiple splicing isoforms are expressed in the adult mouse heart (Fig. 2B). Isoform 2 (exons 1–24) consists of four N-terminal spectrin repeats, three coiled-coil motifs, two central spectrin repeats, and C-terminal Ig and transmembrane domains. In contrast, isoform 1 (exons 1–23) lacks the transmembrane domain and part of the Ig domain. Quantitative PCR (Fig. 2C) and western blot using N- and

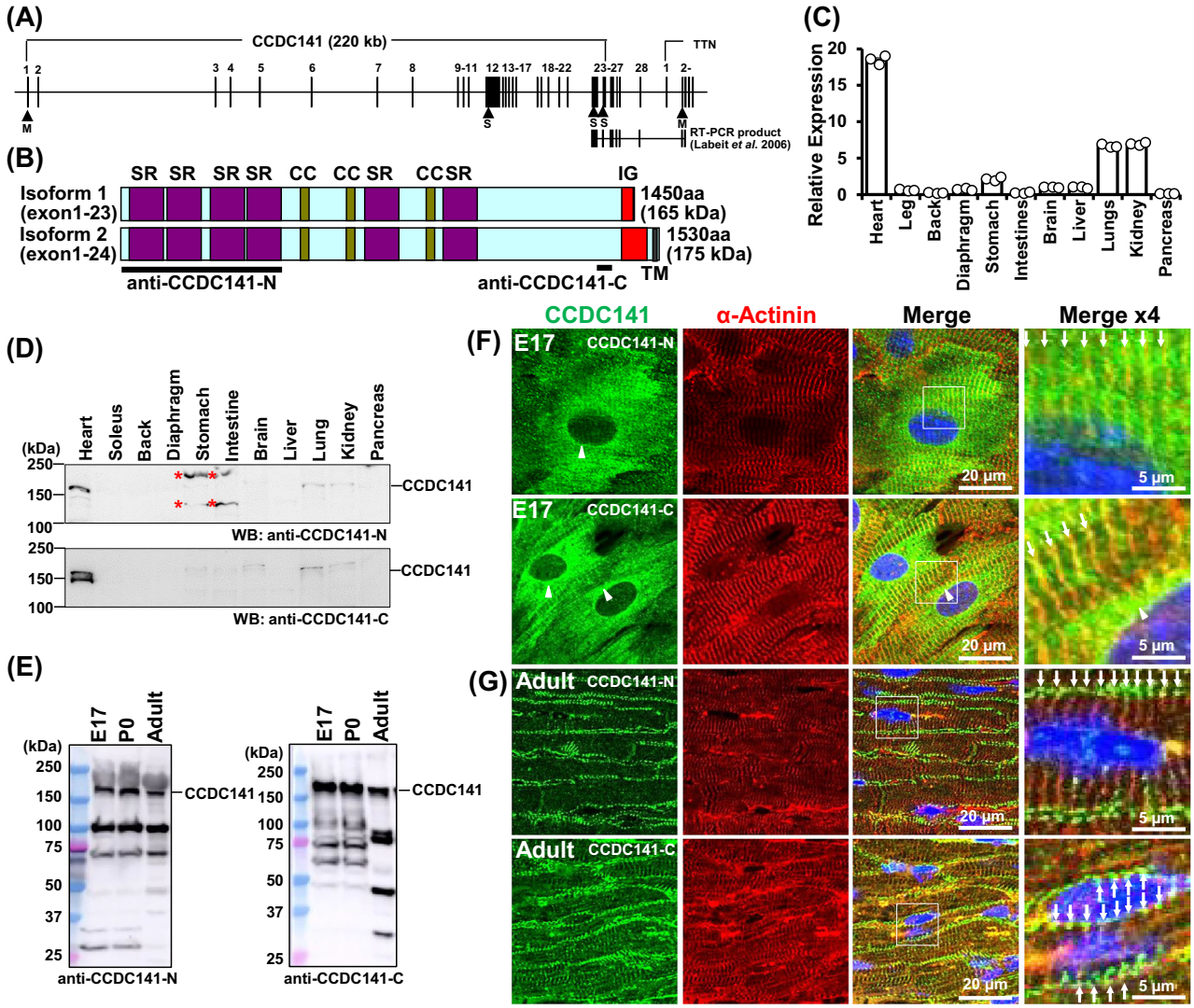

Fig. 2 | CCDC141 is highly expressed in cardiomyocytes. A Gene structure of CCDC141. The human CCDC141 gene spans 220 kb, contains 24 exons, and is located upstream of the connectin gene. An RNA transcript spanning the *CCDC141-TTN* region has been identified (Labeit et al., 2006[10]). 'M' indicates the initiating methionine at the start codon, while 'S' marks a position where a stop codon is present. **B** Domain structures of CCDC141 isoforms. Boxes indicate spectrin repeats (purple), coiled-coil motif (ocher), Ig domain (red), and transmembrane domain (black). Bar indicates epitopes recognized by CCDC141-N and CCDC141-C antibodies. **C** Quantitative PCR analysis of CCDC141 expression across mouse tissues. CCDC141 is highly expressed in the heart. Forward primers target exon 21 and reverse primers target exon 22. Data are presented as mean ± SE. $n = 3$. Endogenous control: 18*S rRNA*. **D** Western blot detection of CCDC141 across mouse tissues using CCDC141-N and CCDC141-C antibodies. Asterisks indicate bands resulting from non-specific antibody binding. **E** Western blot analysis of CCDC141 expression in embryonic (E17), postnatal (P0), and adult hearts using CCDC141-N and CCDC141-C antibodies. **F** Immunofluorescence microscopy showing CCDC141 localization in mouse embryonic (E17) myocardium, using CCDC141-N and CCDC141-C antibodies and counterstained with α-actinin antibody and DAPI. Arrowheads indicate perinuclear localization, while arrows indicate the Z-lines. Boxes mark regions used for Merge ×4 magnified images. **G** Immunofluorescence microscopy of CCDC141 localization in adult mouse myocardium using CCDC141-N and CCDC141-C antibodies, counterstained with α-actinin antibody and DAPI. Arrows indicate the costameres. Boxes mark regions used for Merge ×4 magnified images.

C-terminal CCDC141 antibodies (Fig. 2D) demonstrate high expression in the heart, with moderate levels in the lung and kidney. In fetal mouse hearts, full-length and several smaller CCDC141 are detected by western blot (Fig. 2E). Immunofluorescence microscopy reveals endogenous CCDC141 localization to the Z-line, nuclear envelope, and endoplasmic reticulum in embryonic day 17 cardiomyocytes (Fig. 2F), and primarily to costameres in adult hearts, with weaker signals at the intercalated disc and Z-line (Fig. 2G). To further investigate subcellular localization, EGFP-tagged CCDC141 isoforms were expressed in neonatal rat cardiomyocytes using a mammalian baculovirus system (Fig. 3). After one day in culture, isoform 1 localized near the sarcomere M-line or A-band (Fig. 3A, B) and at the intercalated disc (Fig. 3C), whereas isoform 2 was observed at the nuclear envelope (Fig. 3D) and near the Z-line (Fig. 3E, F). These findings suggest that CCDC141 primarily localizes to costameres in adult cardiomyocytes, with its subcellular distribution modulated by developmental stage, cellular context, and isoform expression.

CCDC141-KO hearts exhibit normal structure and function

To investigate the cardiac role of CCDC141, we analyzed KO mice [$CCDC141^{tm1.1(KOMP)Wtsi}$] generated in the Knockout Mice Program (KOMP) repository at UC Davis (Fig. S1). Exons 3 and 4 of the CCDC141 gene were replaced with the LacZ gene via homologous recombination to express the CCDC141 exon1-exon2-LacZ-polyA (Fig. S1A). Computed tomography showed no change in external appearance (Fig. S1B) or skeletal morphology (Fig. S1C), and genotyping indicated a slightly higher frequency of KO offspring (Fig. S1D). Successful KO and LacZ expression in each tissue were

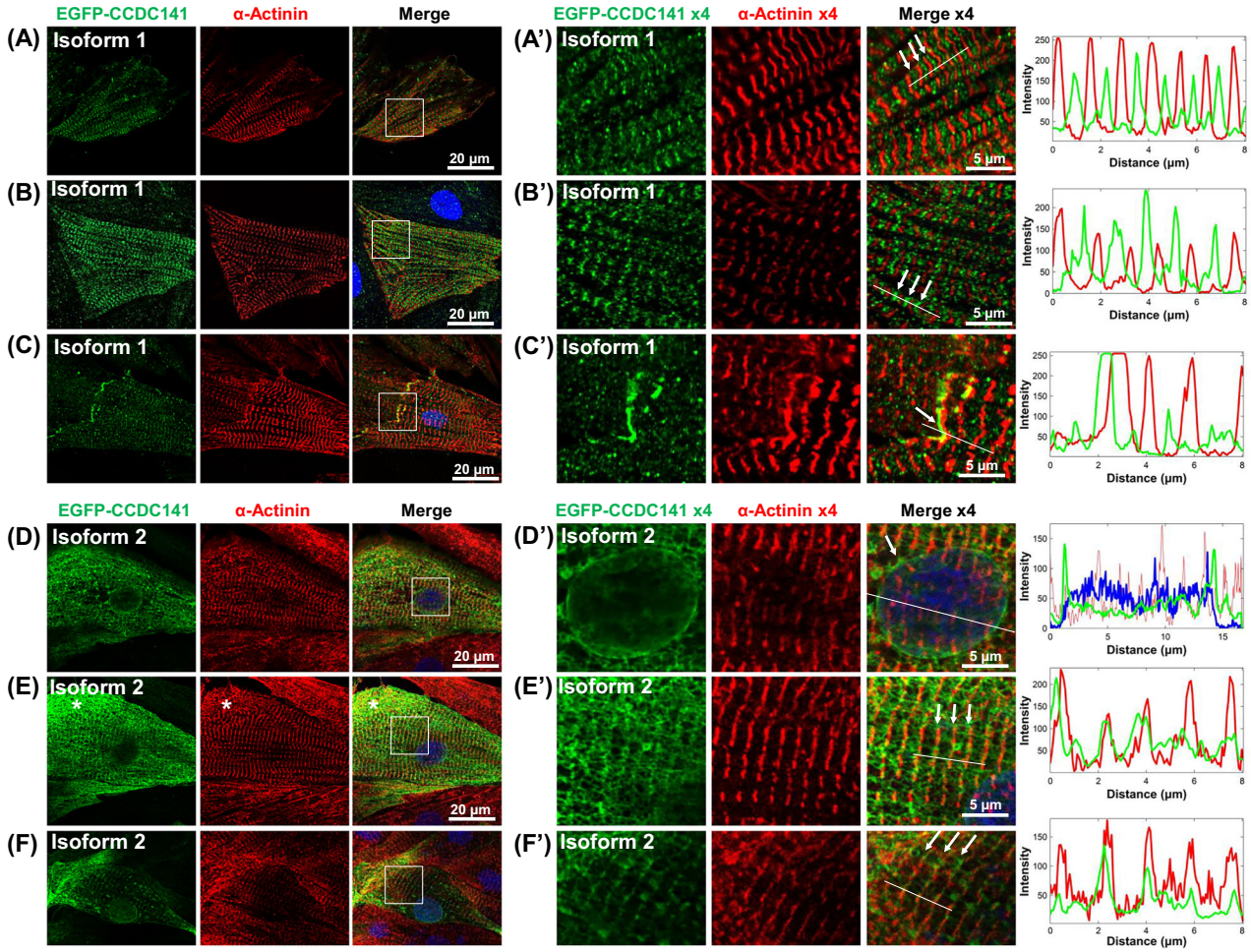

Fig. 3 | CCDC141 isoforms show distinct localization in transfected neonatal cardiomyocytes. EGFP-tagged CCDC141 isoforms were expressed in neonatal rat cardiomyocytes and visualized using GFP antibody and counterstained with α-actinin antibody and DAPI. **A**–**C** Transfection of CCDC141 isoform 1. Boxed regions indicate areas shown at ×4 magnification in panels (**A**'–**C**'). Arrows highlight CCDC141 localization near the sarcomere M-line or A-band (**A**', **B**'), and intercalated disc (**C**'). Thin white lines indicate the positions of the fluorescence intensity linescan plots shown in panel (**A**'–**C**'). **D**–**F** Transfection of CCDC141 isoform 2. A cardiomyocyte was observed from the outer surface (**D**) and interior (**E**). Boxed regions indicate areas shown at ×4 magnification in panels (**D**'–**F**'). Arrows highlight CCDC141 localization at the nuclear envelope (**D**'), near the Z-line with network structure (**E**'), and at the Z-line (**F**'). Thin white lines indicate the positions of the fluorescence intensity linescan plots shown in panel (**D**'–**F**'). The asterisk in panel (**E**) marks a region of CCDC141 accumulation during sarcomere formation.

confirmed by qPCR and western blot (Fig. S1E, S1F). We next analyzed the CCDC141-KO hearts (Fig. S2). Phase-contrast X-ray CT imaging of unfixed hearts revealed no anatomical abnormalities in the left ventricle, including the position and shape of two papillary muscles (Fig. S2A). Echocardiography and telemetry showed normal left ventricular dimensions (Fig. S2B, C), heart rate (Fig. S2D), and electrocardiographic patterns and waveforms (Fig. S2E, F). Thus, CCDC141-KO hearts exhibit normal structure and function.

CCDC141-KO myocardium exhibits cardiomyocyte hypertrophy and altered integrin signaling

We next investigated the CCDC141-KO myocardium. Masson-Trichrome staining showed no significant differences in myocardial density or collagen (blue), muscle (red), and nuclear distribution (purple-black) (Fig. 4A, B). Immunofluorescence microscopy confirmed the absence of CCDC141 at the costamere in KO cardiomyocytes (Fig. 4C, D). Notably, KO cardiomyocytes displayed significant hypertrophy, with increased cross-sectional area (KO 356 vs. WT 288 μm^2, Fig. 4E). However, the localization of cardiomyocyte structural markers, including filamin (costamere), connectin (sarcomere), and nesprin-1 (nuclear envelope), remained unaffected (Fig. S3A, B). Quantitative PCR showed stable expression of *MYH6*, *ACTN2*, and *TCAP*, alongside >2-fold upregulation of connectin (Fig. S4A), while its ratio to myosin heavy chain remained unchanged by SDS-vertical agarose gel electrophoresis (Fig. S4B, C). RNA-seq and KEGG pathway analysis indicated altered focal adhesion and PI3K-Akt pathways (Fig. S5A, B). GO enrichment analysis pointed to roles in angiogenesis, heart development, and extracellular matrix (Fig. S5C). Comprehensive qPCR analysis of focal adhesion-related genes showed reduced expression of integrin subunits *Itga2*, *Itga4*, *Itgb3* (Fig. S5D). Furthermore, western blot of PI3K-Akt signaling components revealed the decreased phosphorylation of upstream PI3K regulators PDK1 and PTEN, while Akt signaling remained unchanged (Fig. S5E, F). These results suggest that CCDC141 deficiency induces cardiomyocyte hypertrophy and potentially changes integrin-mediated signaling from costameres through PI3K independently of Akt.

CCDC141-KO cardiomyocytes disrupt mitochondrial structure and respiration

We examined the mitochondria in CCDC141-KO myocardium (Fig. 5). Immunohistochemistry and electron microscopy revealed mitochondrial aggregation and fusion in KO myocardium, with increased cross-sectional area (KO 1.23 vs. WT 0.78 μm^2, Fig. 5A–C). In contrast, qPCR and western blot showed unchanged expression level of mitochondrial markers COXIV (COX4i1) and mitofusin-2 (Fig. 5D–F). To evaluate mitochondrial metabolism, we measured

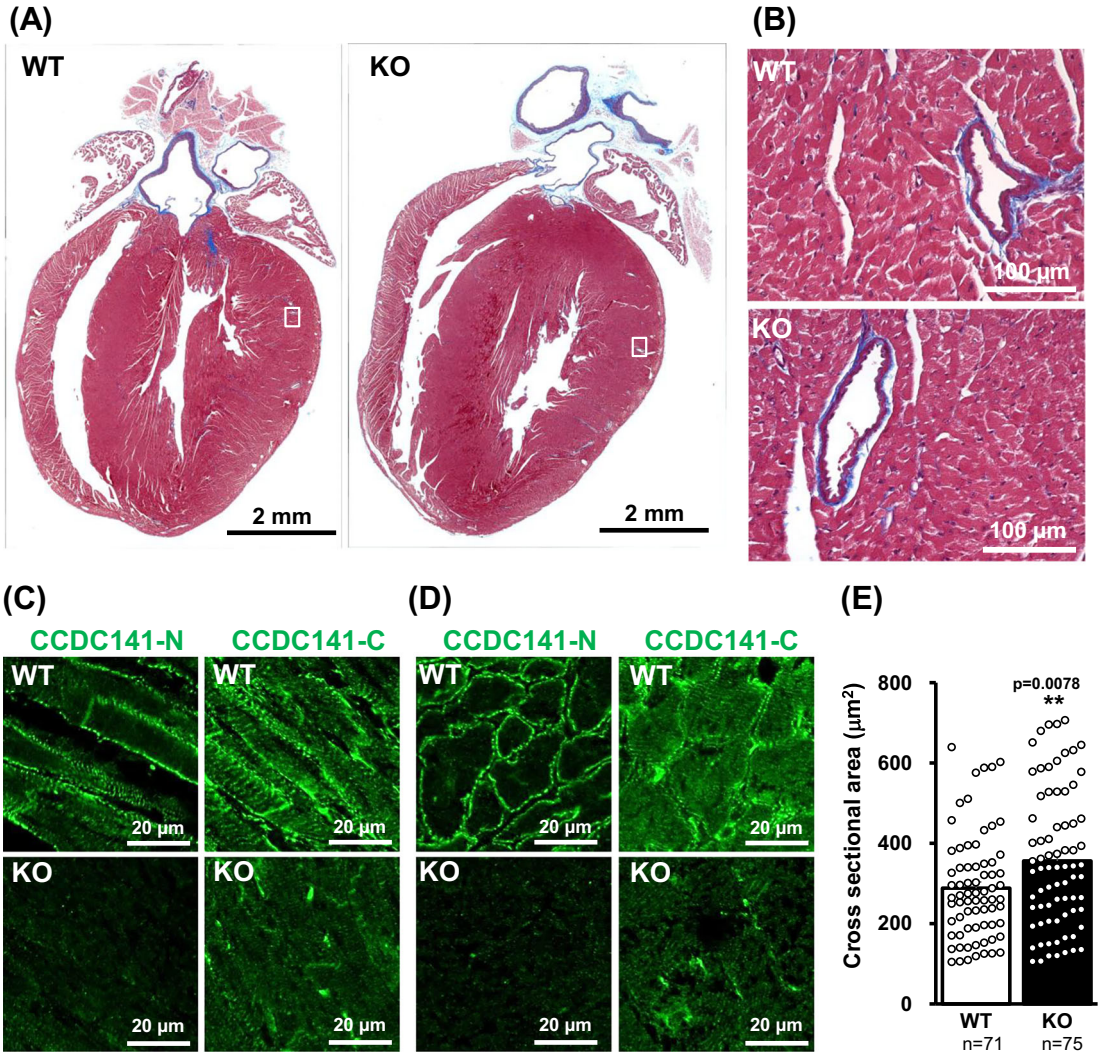

Fig. 4 | CCDC141-KO myocardium exhibits cardiomyocyte hypertrophy. **A** Masson's Trichrome staining of heart sections from wild-type and CCDC141-KO mice. **B** Enlarged view of the boxed region in (**A**). **C**, **D** Immunofluorescence microscopy showing CCDC141 localization in longitudinal (**C**) and transverse (**D**) myocardial sections of CCDC141-KO hearts. **E** Quantification of cardiomyocyte cross-sectional area from immunofluorescence images of transverse sections. CCDC141-KO cardiomyocytes exhibit hypertrophy. ** indicates $p < 0.01$.

oxygen consumption rate (OCR) in isolated KO cardiomyocytes under basal respiration, ATP synthesis inhibition by oligomycin, expedited proton circuit and electron flow by FCCP, and inhibited proton circuit by rotenone/antimycin A (Fig. 5G). CCDC141-KO cardiomyocytes displayed a stressed metabolic phenotype, characterized by sustained high ATP demand, ~2-fold increased basal OCR, and ~3-fold higher ATP production. While maximal respiratory capacity was unaffected, spare respiratory capacity was markedly reduced (Fig. 5H). These results suggest that CCDC141 deficiency impairs mitochondrial structural integrity and limits homeostatic flexibility in cardiomyocytes.

CCDC141-KO cardiomyocytes enhance Ca^{2+} handling via SERCA2a upregulation

We next investigated contraction dynamics, Ca^{2+} kinetics, and associated regulatory proteins in isolated CCDC141-KO cardiomyocytes (Fig. 6A). Contraction responses in stimulation at 0.5, 1, 2, and 4 Hz showed no significant differences (Fig. 6B). In contrast, transient Ca^{2+} measurements revealed marked changes in kinetic profiles (Fig. 6C): basal Ca^{2+} content remained unchanged (Fig. 6D), but the rate of Ca^{2+} increase was approximately 1.6-fold higher in CCDC141-KO cardiomyocytes (Fig. 6E). Time to peak Ca^{2+} was unchanged (Fig. 6F), while both the time required for Ca^{2+} decline to half-maximal level (Fig. 6G) and the time to constant Ca^{2+} level (Fig. 6H) were significantly shortened. Sarcoplasmic reticulum Ca^{2+} storage was 2.3-fold higher in CCDC141-KO cardiomyocytes (Fig. 6I). qPCR analysis revealed that NCX1, which exports Ca^{2+} to the extracellular fluid, was 1.8-fold higher in the CCDC141-KO myocardium, RyR2, which releases Ca^{2+} from the SR, was 1.2-fold higher, SERCA2a, which recovers Ca^{2+} to the SR, was 1.5-fold higher, and PLN, which modulates SERCA2a activity, was 1.5-fold higher (Fig. 6J). Western blot further confirmed enhanced SERCA2a protein levels (Fig. 6K). Thus, CCDC141-KO cardiomyocytes displayed enhanced Ca^{2+} handling due to increased SERCA2a.

CCDC141-KO hearts exhibit low tolerance to mechanical stress

Finally, we performed transverse aortic constriction (TAC) surgery to analyze the effects of pressure overload on the heart (Fig. 7). In wild-type, hearts demonstrated severe myocardial fibrosis six months post-TAC (Fig. 7A), with CCDC141 prominently localized at the nuclear envelope of cardiomyocytes (Fig. 7B and Fig. S6). In contrast, most CCDC141-KO mice died within hours to days after TAC, and electrocardiographic recordings captured the sudden onset of lethal arrhythmias immediately prior to death (Fig. 7C). To reduce surgical severity, we used a 25-gauge needle in place of the standard 27-gauge and performed moderate TAC. Although over half of the CCDC141-KO mice died within a few days, some mice survived beyond

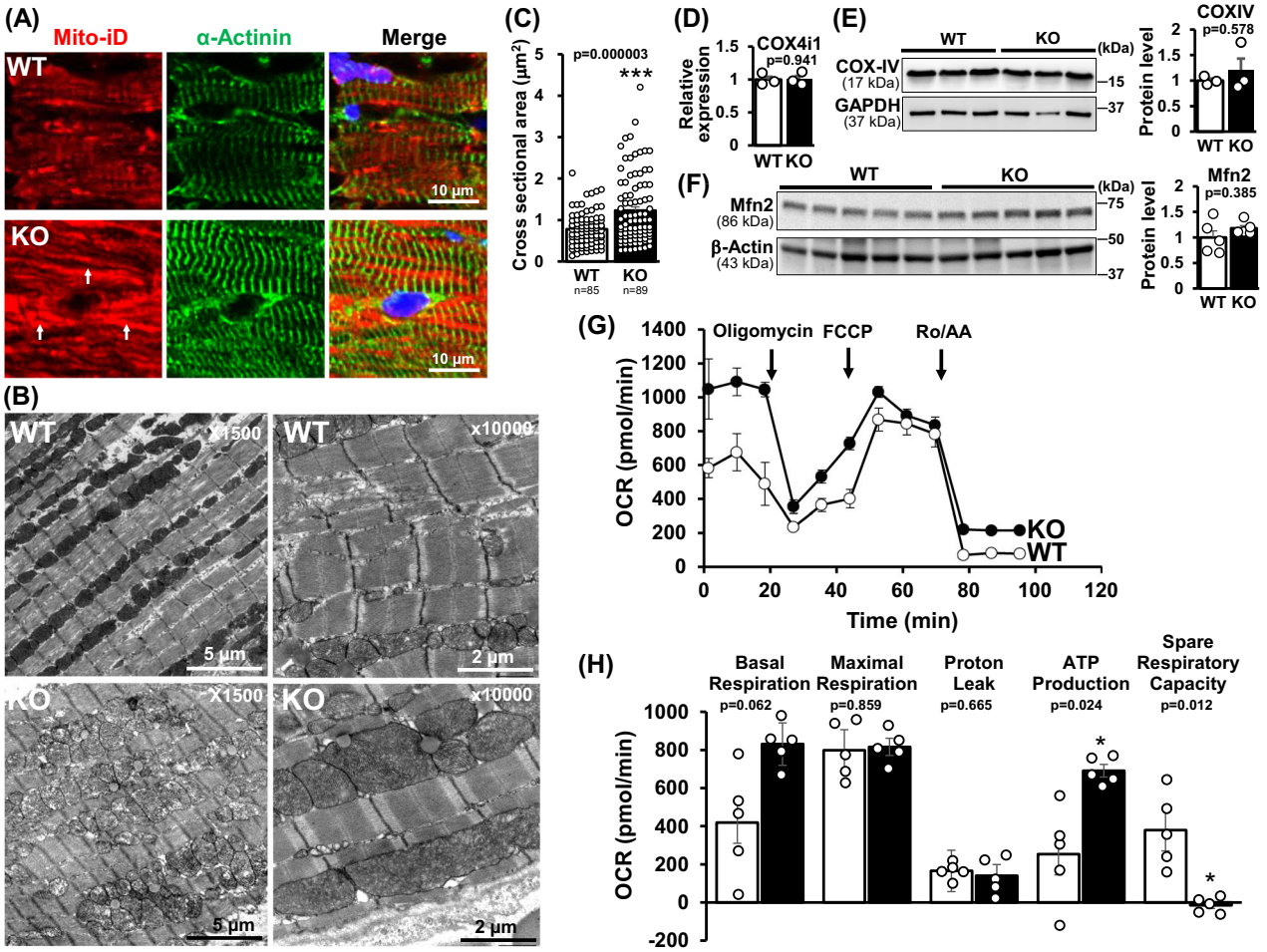

Fig. 5 | CCDC141-KO cardiomyocytes disrupt mitochondrial structure and respiration. A Immunofluorescence microscopy of CCDC141-KO myocardium stained with mito-iD and counterstained with α-actinin and DAPI. Arrows indicate mitochondrial aggregation and loss of striated localization in the CCDC141-KO myocardium. **B** Electron microscopy of CCDC141-KO myocardium. Mitochondrial alignment and size were disrupted in the CCDC141-KO myocardium. **C** Quantification of mitochondrial cross-sectional area based on EM images in (**B**). *** indicates $p < 0.001$. **D** Quantitative PCR analysis of the COXIV gene (*COX4i1*) in CCDC141-KO hearts. Mean ± SE. $N = 3$, $n = 2$. Endogenous control: 18*S rRNA*. **E** Western blot analysis of the mitochondrial marker protein COXIV. $N = 3$, $n = 2$. **F** Western blot analysis of the mitochondria fusion protein Mfn2. $N = 5$. Expression levels of COXIV and Mfn2 remained unchanged. **G** Mitochondrial respiration analysis in isolated CCDC141-KO cardiomyocytes. Mean ± SE. $n = 5$. **H** Summary graph of indicators of mitochondrial respiration. Mean ± SE. $n = 5$. CCDC141-KO cardiomyocytes lacked spare respiratory capacity. * indicates $p < 0.05$.

3 months (Fig. 7D). However, these surviving KO mice exhibited markedly impaired cardiac function with reduced fractional shortening on echocardiography (Fig. 7E, F). Histological analysis with Masson's trichrome staining revealed severe cardiac hypertrophy and extensive fibrosis, particularly in peripheral myocardial regions (Fig. 7G). Furthermore, electron microscopy of left ventricular cardiomyocytes showed abnormal nuclear morphology and absence of endoplasmic reticulum (Fig. 7H). Therefore, CCDC141-KO hearts have low tolerance to mechanical stress and are more susceptible to fatal arrhythmias and progressive heart failure.

Discussion

Our findings identify CCDC141 as a binding partner of connectin and nesprin-1, and localizes to the costameres of adult cardiomyocytes. In CCDC141-KO hearts, mitochondrial metabolism and Ca^{2+} dynamics were significantly altered. Under mechanical stress-induced heart failure, CCDC141 was redistributed to the nuclear envelope. Its absence increased susceptibility to lethal arrhythmogenesis and progressive heart failure under mechanical stress.

Connectin functions as a scaffold for mechanosensitive proteins, triggering signaling in response to mechanical load[3]. Here, we showed that the Ig domain of CCDC141 binds to connectin (Fig. 1A–C), similar to other connectin-binding proteins such as obscurin, c-protein, filamin, myomesin, tcap, and myopalladin. When CCDC141 isoform 1 (connectin-binding isoform) was transfected into neonatal rat cardiomyocytes, it located near the M-line (Fig. 3). The connectin C-zone, a binding site for CCDC141 (Fig. 1A, C), also associates with myosin filaments. CCDC141 interacts with phosphorylated myosin-regulatory light chains[20], whose phosphorylation enhances myocardial contractility and Ca^{2+} sensitivity[21]. Therefore, CCDC141 localization to the C-zone potentially affect both contractile function and Ca^{2+} sensitivity. The connectin P-zone, another binding site for CCDC141 (Fig. 1A, C), also interacts with MuRF1 and MuRF2, key regulators of muscle mass and metabolism[22]. Remarkably, cardiomyocyte hypertrophy (Fig. 4) and mitochondrial alterations (Fig. 5A, B) in CCDC141-KO hearts resemble the MuRF1/MuRF2 double KO phenotypes[23]. Therefore, MuRFs may contribute to changes observed in CCDC141-KO hearts.

Nesprin forms the LINC complex with SUN proteins at the nuclear envelope, transmitting extracellular mechanical signals to the nucleus and modulating gene expression to adapt to mechanical loading[6]. We showed that the spectrin repeats of CCDC141 bind to those of nesprin-1 (Fig. 1E, F). CCDC141 localized to the nuclear envelope upon transfection into neonatal rat cardiomyocytes (Fig. 3) and under pressure overload-induced

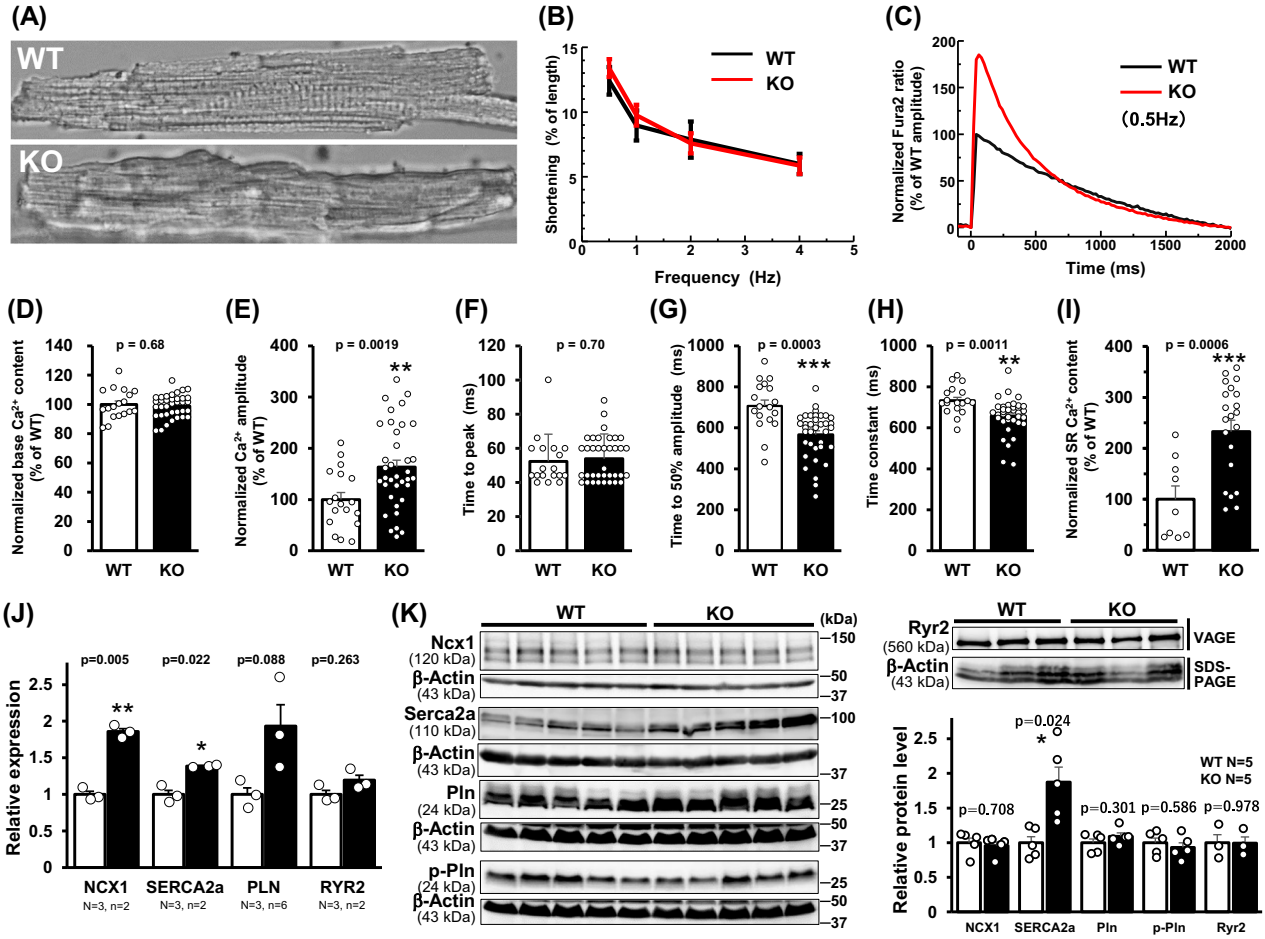

Fig. 6 | CCDC141-KO cardiomyocytes enhance Ca^{2+} handling via SERCA2a upregulation. **A** Microscopic observation of isolated cardiomyocytes. **B** Contraction rate of CCDC141-KO cardiomyocytes stimulated at 0.5, 1, 2, or 4 Hz. No significant differences were observed. Mean ± SE. WT: $N = 3$, $n = 14$; KO: $N = 4$, $n = 33$. **C–I** Ca^{2+} transients in CCDC141-KO cardiomyocytes. Mean ± SE. WT: $N = 3$, $n = 18$; KO: $N = 4$, $n = 36$. **C** A typical example of Ca^{2+} transient trace. **D** Basal Ca^{2+} content. **E** Rate of Ca^{2+} increase during electrical stimulation. **F** Time to peak Ca^{2+} increase. **G** Time to half-maximal Ca^{2+} exhaust. **H** Times to constant Ca^{2+} level. **I** Ca^{2+} content in the sarcoplasmic reticulum. CCDC141-KO cardiomyocytes showed enhanced Ca^{2+} storage and Ca^{2+} transient dynamics of SR. *** indicates $p < 0.001$. ** indicates $p < 0.01$. **J** Quantitative PCR analysis of Ca^{2+} regulatory proteins. Mean ± SE. $N = 3$, $n = 2$. Endogenous control: GAPDH (for NCX1, SERCA2a, and RYR2), 18*SrRNA* (for PLN). ** indicates $p < 0.01$. * indicates $p < 0.05$. **K** Western blot analysis of Ca^{2+} regulatory proteins. Mean ± SE. RyR2 ($N = 3$) was separated using SDS-vertical agarose gel electrophoresis, and all others ($N = 5$) were separated using SDS-PAGE. Increased SERCA2a improved Ca^{2+} recovery in the SR. * indicates $p < 0.05$.

heart failure (Fig. 7B). In CCDC141-KO hearts, even moderate pressure overload led to nuclear morphology defects and accelerated progression to heart failure (Fig. 7H), suggesting that the CCDC141–nesprin-1 interaction is essential for cardiac nuclear mechanotransduction. These findings highlight CCDC141 as a key regulator of nuclear adaptation to mechanical stress.

Costameres connect integrins on the cardiomyocyte membrane to sarcomere Z-lines. Spectrin family proteins, including spectrin, dystrophin, and α-actinin, form a structural network within the costamere. CCDC141 contains spectrin repeats and localizes to costameres (Fig. 2B, G), suggesting its participation in this network. In CCDC141-KO hearts, Itgb3 expression was reduced (Fig. S5D), PTEN and PDK1 phosphorylation were decreased (Fig. S5F), and cardiomyocytes exhibited hypertrophy (Fig. 4E). These findings align with reports that Itgb3 regulates the PTEN pathway in cardiomyocytes[24]. Furthermore, CCDC141-KO hearts developed heart failure even under moderate pressure overload (Fig. 7D–H), consistent with the observation that Itgb3-KO hearts undergo calpain-mediated cardiomyocyte death even under moderate pressure overload[25]. Thus, CCDC141 localizes to costameres and may contribute to integrin-mediated mechanical stress transmission and the development of pressure overload-induced heart failure.

Mitochondria bind directly to microtubule tubulin, facilitating their migration, fusion, and fission. We demonstrated that CCDC141-KO hearts exhibit altered mitochondrial alignment, morphology, and metabolism (Fig. 5). Because CCDC141 deficiency affects tubulin integrity[26], these mitochondrial irregularities may result from microtubule instability (Fig. 5). Microtubule-dependent mitochondrial alignment regulates Ca^{2+} release in response to nanomechanical stimulus[27]. Furthermore, mitochondria modulate cardiomyocyte Ca^{2+} homeostasis by producing reactive oxygen species (ROS), which exert protective effects during the preischemic phase[28]. However, excess ROS impairs intracellular Ca^{2+} dynamics through RyR2 leakage and SERCA2a nitration, resulting in lethal arrhythmias and heart failure. Increased oxidative stress due to excess ROS alters cardiomyocyte stiffness through disulfide bond formation and phosphorylation of the connectin N2B region and glutathionylation of the connectin Ig domain[3]. Therefore, mitochondrial irregularities likely underlie the Ca^{2+} dynamic changes (Fig. 6C–I) and lethal arrhythmias (Fig. 7C) observed in CCDC141-KO hearts.

CCDC141-KO hearts increased SERCA2a expression, Ca^{2+} release from SR, and Ca^{2+} recovery to SR (Fig. 6). The results of the Ca^{2+} transients showed that the amplitude was higher and the decay was faster in KO mice compared to wild type (Fig. 6E, G, H). These changes are similar to the

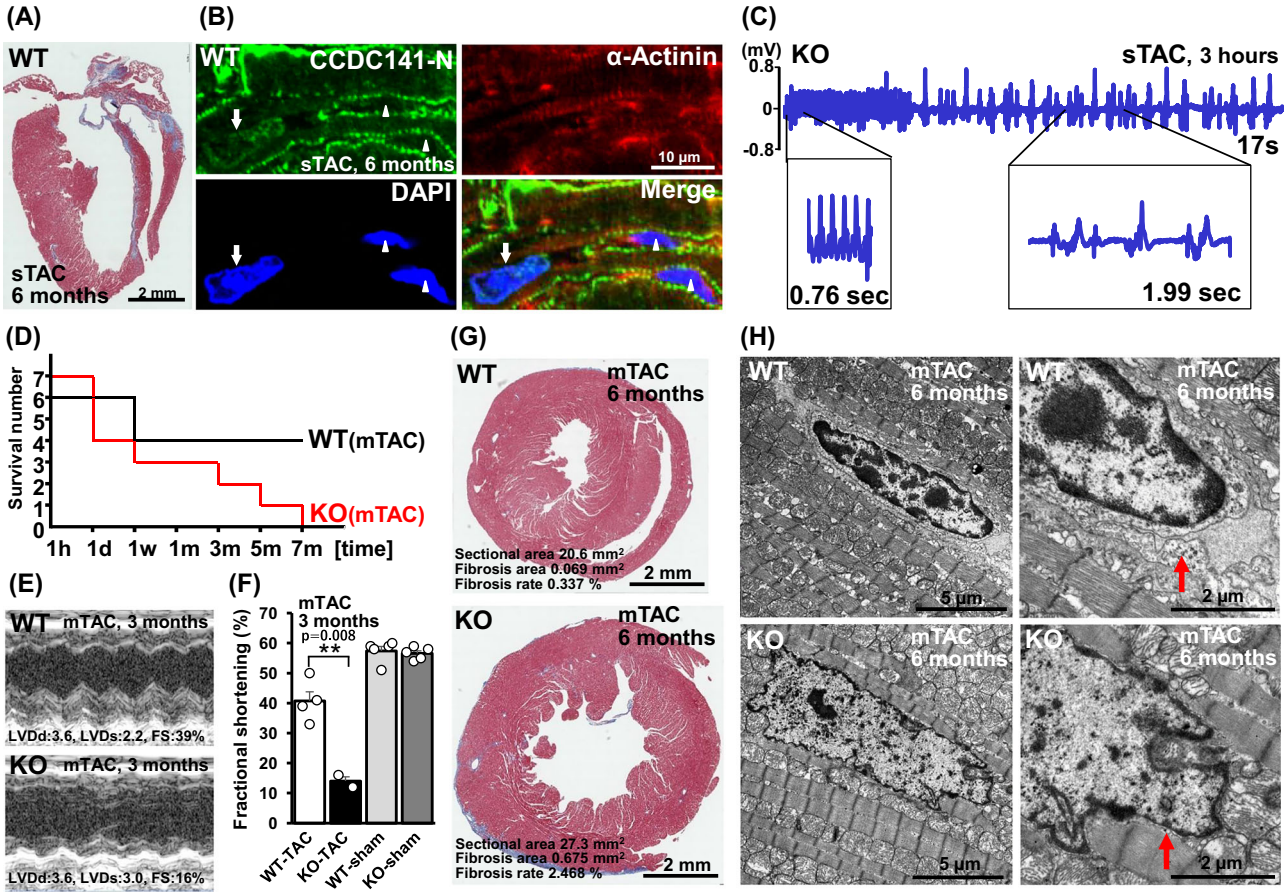

Fig. 7 | CCDC141-KO hearts exhibit low tolerance to mechanical stress. **A** Masson's Trichrome staining of wild-type hearts 6 months after severe transverse aortic constriction (sTAC) surgery. **B** Immunofluorescence microscopy of adult myocardium 6 months after sTAC, stained with CCDC141-N antibody and counterstained with α-actinin and DAPI. Arrows indicate nuclear localization of CCDC141 in cardiomyocyte nuclei. Arrowheads indicate nuclei of non-cardiomyocytes. **C** Electrocardiogram recording of CCDC141-KO mouse immediately prior to sudden death following sTAC surgery. **D** Survival analysis of CCDC141-KO mice after moderate TAC (mTAC) surgery. WT, $N = 6$. KO, $N = 7$. **E** Representative echocardiographic images of CCDC141-WT and KO hearts that survived for more than 3 months post-mTAC. **F** Fractional shortening of hearts that survived beyond 3 months after mTAC or sham surgery. WT-TAC, $N = 4$. KO-TAC, $N = 2$. WT-sham, $N = 5$. KO-sham, $N = 5$. ** indicates $p < 0.01$. **G** Masson's Trichrome staining of CCDC141-KO hearts 6 months after mTAC surgery. **H** Electron microscopy of CCDC141-KO hearts 6 months post-mTAC. Arrows indicate presence (WT) and absence (KO) of endoplasmic reticulum. CCDC141 deficiency induces cardiac failure associated with nuclear morphology disruption.

effects induced by catecholamines. On the other hand, no significant difference was observed in the extent of shortening in isolated unloaded cardiomyocytes (Fig. 6B), nor in the fractional shortening of beating whole hearts (Fig. S2B, C). These phenomena may be caused by a decrease in the Ca^{2+} sensitivity of myofilaments. The increased ATP production in KO mice (Fig. 5H) appears to be used for Ca^{2+} handling rather than for external mechanical work, which is similar to pathological conditions such as hyperthyroidism[29] and cardiac acidosis[30]. Although cardiac function appears normal under physiological load in KO mice, it is likely sustained by compensatory mechanisms, implying that these mice may be susceptible to excessive pressure overload (Fig. 7).

CCDC141-KO hearts developed lethal arrhythmias shortly after TAC surgery (Fig. 7C). Genome-wide association studies have linked CCDC141 to various cardiac traits, including heart rate[11], QT interval[12], QRS duration[13], QRS complex of the ECG[14], blood pressure[15,16], supraventricular Arrhythmias[18], and bradyarrhythmia development[19]. In particular, prolonged QT interval implies delayed myocardial repolarization and is a risk factor for ventricular arrhythmias and sudden cardiac death (SCD), and its associated genes are strongly involved in the Ca^{2+} signaling pathway[12]. In CCDC141-KO hearts, altered Ca^{2+} dynamics likely impair adaptive responses to acute ischemia and blood pressure changes induced by TAC, predisposing to SCD from lethal arrhythmias (Fig. 7C). This vulnerability may stem from impaired blood pressure regulation, defective cardiac electrophysiological modulation via QT interval-related genes, and reduced mitochondrial reserve respiratory capacity (Fig. 5G, H).

This study found that CCDC141 binds to the connectin C-zone and P-zone on myosin filaments (Fig. 1A–C) and localizes to costameres on the sarcomere Z-line (Fig. 2G). Its ortholog in *Drosophila*, Zormin, exhibits similar localization at the Z-line, M-line, and thick filament ends, as shown by immunofluorescence and immuno-electron microscopy[31]. Zormin also binds to actin and myosin[31] and may interact with obscurin at the M-line[32], supporting an evolutionarily conserved role shared by CCDC141 and Zormin. In CCDC141-KO hearts, connectin mRNA expression was elevated (Fig. S4A). While CCDC141 and connectin are transcribed from separate genes in mammals, joint transcription events of FLJ39502 (a tentative name of CCDC141)-TTN[10] (Fig. 1A) suggest potential isoform relationships, similar to the *Drosophila* Sls gene, which encodes both Zormin and D-Titin isoforms[31]. This suggests a cooperative mechanism resembling the operon-like regulation in *E. coli* via RNA linkage and protein interaction. Supporting this, the ancestral gene "connectitin" (connected-connectin/titin), had integrated structure of three adjacent genes, *SESTD1-CCDC141-CON(TTN)*[33]. Conservation across humans and *Drosophila* (diverged ~600 million years ago), and CCDC141 mutations in extinct Neanderthals[34], point to critical survival roles. In mice, CCDC141 knockout caused sudden

death or heart failure under stress (Fig. 7), reinforcing its essential function for survival under various stresses in the natural environment.

CCDC141, a novel binding protein of connectin and nesprin-1, localizes to costameres in adult cardiomyocytes and to the nuclear envelope during heart failure. CCDC141-KO hearts exhibit impaired mitochondrial metabolism and altered Ca^{2+} handling, rendering them vulnerable to stress. These findings provided new insights into the molecular basis of cardiac mechanoadaptation and disease.

Methods

Animals

CCDC141 knockout (KO) mice were generated through the Knockout Mice Program (KOMP) at the University of California, Davis (Project ID# CSD74901). C57BL/6N-CCDC141$^{tm1.1(KOMP)Wtsi}$ mice sperm were used to fertilize oocytes from a C57BL/6 N Crl background. The resulting offspring were genotyped by PCR using genomic DNA extracted from their tails. To compare, wild-type and KO mice offspring from crossing heterozygous parents were employed. Mice were housed in standard cages (3–5 animals per cage) under a conventional 12-h light/dark cycle. Anesthesia was induced with sevoflurane and maintained using a combination of medetomidine hydrochloride, midazolam, and butorphanol tartrate. Euthanasia was performed by sevoflurane overdose. The number of animals used was the minimum required to achieve statistical significance. Experimental units were not randomized, and no control groups were included to minimize potential confounding variables. Blinding was not implemented at any stage of the experiments. Sample size was not determined based on outcome measures or power calculations. All procedures involving animals were conducted in accordance with the guidelines of the Animal Committee at Kawasaki Medical School. We affirm compliance with all relevant ethical regulations governing animal research.

Transverse aortic constriction (TAC) surgery

Mice aged 15–30 weeks were anesthetized using a mixture of three anesthetics, including medetomidine hydrochloride (Domitor®; Nippon Zenyaku Kogyo, Japan), midazolam hydrochloride (Dormicum®; Maruishi Pharma, Japan), and butorphanol tartrate (Vetorphale®; Meiji Seika Pharma, Japan) at 0.3, 4.0, and 5.0 mg/kg body weight, respectively. After orotracheal intubation, the cannulae were connected to a volume cycle ventilator (SN-480-7; Shimano, Japan) delivering room air with a 0.2 mL tidal volume and a respiratory rate of 110 breaths/minute. A small incision was made in the second intercostal space to expose the thoracic cavity. The transverse aorta was constricted by ligation using a 7-0 nylon string with a blunted 25-gauge (moderate constriction) or 27-gauge (severe constriction) needle, which was immediately removed. Atipamezole hydrochloride (Atipame®; Kyoritsu Seiyaku, Japan) at 3.0 mg/kg body weight was used to reverse anesthesia. After surgery, the mice were kept at rest at 37 °C. Survival analysis was performed on individuals that lived for more than one hour: 3 males and 3 females from the WT group, and 6 males and 1 female from the KO group. Among these, echocardiography was conducted on mice that survived beyond three months, comprising 2 males and 2 females from the WT group and 2 males from the KO group. Histological analysis was subsequently performed on the male mice that survived up to six months. Sham TAC surgery was performed on five male WT mice and five male KO mice, all of which survived for more than three months and underwent echocardiographic evaluation.

Echocardiography

Cardiac function was evaluated by two-dimensional transthoracic echocardiography using the Aplio300 system with a 14 MHz transducer (Toshiba Medical System, Japan), as previously described[35,36]. Male mice were anesthetized with 2% sevoflurane and maintained under 1% sevoflurane throughout the examination. Left ventricular internal diameters at the end-diastole (LVDd) and end-systole (LVDs) were measured using M-mode imaging. Fractional shortening (FS) was calculated as $\{(LVDd\text{-}LVDs) / LVDd\}$ x 100 (%) and used as an index of cardiac contractile function.

ECG telemetry

Electrocardiograms (ECGs) were continuously recorded as previously described[36]. Male mice were anesthetized with 3% sevoflurane, and a telemetry transmitter device (Physiol Tel® HD-X11, Data Sciences International, USA) was implanted into the peritoneal cavity. Two ECG leads were positioned at the cardiac apex and the right acromion. Conscious mice were housed under 12-h light/dark cycle (on/off, 8 am to 8 pm). ECG traces were continuously recorded every minute for 10 s using Dataquest ART 4.0 software (Data Sciences International, USA) beginning the day after a two-day recovery period. Heart rate was calculated by digitally tracking ECG RR intervals using Dataquest software.

X-ray phase-contrast tomography

Three-dimensional structures of mice hearts (5 WT and 5 CCDC141-KO males) were visualized using X-ray phase-contrast tomography at beamline BL20B2 of the SPring-8 Synchrotron Radiation Facility, Japan, as previously described[37], with approval of the SPring-8 Proposal Review Committee (proposal number: 2023B1523). Mice were deeply anesthetized using isoflurane inhalation, and hearts were excised. A blunted fine needle was cannulated into the aorta, followed by perfusion with phosphate-buffered saline containing 50 mM 2,3-butanedione monoxime (BDM) to induce ventricular relaxation mimicking diastole. The left atrium was ligated, and ultrasound gel (Parker Laboratories, USA) was injected into the left ventricle through an inserted needle via the aorta. Subsequently, the right atrium was ligated, and ultrasound gel was injected into the right ventricle. Left ventricular pressure was adjusted to the physiological range (5-10 mmHg). The heart was placed in an imaging container filled with dissolved 2% agarose, which was cooled to solidify the gel. Phase-contrast CT imaging was performed using an X-ray Talbot interferometer (grating pitch of 4.8 μm) assembled in the third hatch of BL20B2. The X-ray energy was adjusted to 40 keV. The X-ray detector comprised a beam-monitor AA60 and a high-definition CMOS camera ORCA Quest (Hamamatsu Photonics). The effective pixel size was 3.68 μm, and the field of view was 15.1 mm (H) x 8.5 mm (V). 3D visualization was performed using Drishti software[38].

Histochemical analysis, electron microscopy, and immunofluorescence microscopy

For histochemical analysis, hearts were fixed in 4% paraformaldehyde, embedded in paraffin, sectioned at 3 μm thickness, and stained with Masson's trichrome according to standard procedures. Sections were observed using an all-in-one fluorescence microscopy (BZ-X710, Keyence, Japan). For electron microscopy (EM), tissues were fixed with 2.5% glutaraldehyde, post-fixed with 1% osmium tetroxide, dehydrated through a graded ethanol series, and embedded in Epon-Araldite resin (OKEN, Japan). Serial ultrathin sections (60–90 nm thick) were stained with uranyl acetate and lead citrate, and observed using a transmission electron microscope (JEM1400; JEOL, Japan). Immunofluorescence (IF) microscopy was performed as previously described[39,40]. Freshly excised tissues were embedded in Tissue-Tek OCT compound (Sakura Finetek, Japan), frozen, and sectioned at 7-μm using a cryostat (Leica, Germany). Sections were permeabilized with 0.1% Triton-X-100 and blocked with Blocking-One (Nacalai Tesque, Japan). Double-labeling was performed using primary antibodies followed by Alexa Fluor 488- or 568-conjugated secondary antibodies (Thermo-Fisher Scientific, USA). Mitochondria were stained with Mito-iD (Enzo Life Sciences, USA). Sections were mounted with Dako fluorescent mounting medium (Dako, USA) and imaged using a confocal laser scanning microscope (FV1000; Olympus, Japan). Cardiomyocyte cross-sectional area was quantified using ImageJ software based on IF images of vinculin-stained myocardium. Only cardiomyocytes with an area greater than 100 μm^2 were included in the analysis.

Measurement of cell shortening and Ca^{2+} transients

As previously described[41], ventricular cardiomyocytes were enzymatically isolated from adult mice. Briefly, the heart was rapidly excised and perfused using a Langendorff system with cell isolation buffer (CIB, 130 mM NaCl, 5.4 mM KCl, 0.5 mM $MgCl_2$, 0.33 mM NaH_2PO_4, 22 mM glucose, 50 nM/mL bovine insulin, and 25 mM HEPES-NaOH, pH 7.4) containing 0.4 mM EGTA for 3–5 min. This was followed by perfusion for 8–10 min with an enzyme solution (ES, CIB supplemented with 1 mg/mL collagenase type II [Worthington Biochemical, USA], 0.06 mg/mL protease [Sigma-Aldrich, Japan], and 0.06 mg/mL trypsin [Sigma-Aldrich, Japan]) containing 0.3 mM $CaCl_2$. The left ventricles were excised, cut into several pieces, and further digested in ES containing 0.7 mM $CaCl_2$ and 2 mg/mL BSA for 10–15 min at 37 °C with gentle agitation. After centrifugation at 300 rpm for 5 min, the pellet was resuspended in CIB containing 1.2 mM $CaCl_2$ and 2 mg/mL BSA, incubated for 10 min at 37 °C, centrifuged again, and finally resuspended in Tyrode solution (140 mM NaCl, 5.4 mM KCl, 1.8 mM $CaCl_2$, 0.5 mM $MgCl_2$, 0.33 mM NaH_2PO_4, 11 mM glucose, 2 mg/mL BSA, and 5 mM HEPES-NaOH, pH 7.4). Cell shortening and Ca^{2+} transients of isolated cardiomyocytes were measured as previously described[36]. Steady-state conditions at 0.5, 1, 2, and 4 Hz were induced using a two-platinum electrode insert connected to an isolator (SS-104J; Nihon Kohden, Japan) and a bipolar stimulator (SEN-3401; Nihon Kohden, Japan). For Ca^{2+} transients measurements, cardiomyocytes were loaded with 5 μM Fura-2-acetoxymethyl ester (Dojindo, Japan), a Ca^{2+}-sensitive fluorescent dye, as previously described[35]. Fluorescence emission at 510 nm was recorded under alternating excitation at 340 and 380 nm (pE-340^{fura}; CoolLED, UK) during field stimulation at 0.5 Hz. Sarcoplasmic reticulum Ca^{2+} content was evaluated by measuring the peak Ca^{2+} transient following exposure to 10 mM caffeine.

Mitochondrial oxygen consumption rate (OCR) measurement

Cardiomyocytes from adult mice were isolated using a Langendorff-free method[42]. Briefly, mice were euthanized with excessive sevoflurane, and the inferior vena cava was dissected. EDTA buffer (130 mM NaCl, 5 mM KCl, 0.5 mM NaH_2PO_4, 10 mM HEPES, 10 mM glucose, 10 mM BDM, 10 mM taurine, 5 mM EDTA, pH 7.8) was injected into the right ventricle. The heart was excised after clamping the aorta and sequentially treated with EDTA buffer, perfusion buffer (130 mM NaCl, 5 mM KCl, 0.5 mM NaH_2PO_4, 10 mM HEPES, 10 mM glucose, 10 mM BDM, 10 mM taurine, 1 mM $MgCl_2$, pH 7.8), and collagenase buffer (perfusion buffer supplemented with 0.5 mg/mL collagenase type II [Worthington Biochemical, USA], 0.5 mg/mL collagenase type IV [Worthington Biochemical, USA], 0.05 mg/mL protease XIV [Sigma-Aldrich, Japan]) via the apex. The heart was then mechanically dissociated in collagenase buffer. Digestion was arrested by adding the stop buffer (Perfusion buffer containing 5% FBS). Myocytes were filtered through a 100 μm mesh, collected by gravity sedimentation, and resuspended in a perfusion buffer. Mitochondrial OCR was measured using an Extracellular Flux Analyzer XFe24 (Agilent Technologies, USA), following the manufacturer's instructions. FluxPak XFe24 cell culture microplates (Agilent Technologies, USA) were coated with AteroCell IPC-50 (Koken, Japan), and 3000 isolated cardiomyocytes were seeded per well. Cells were incubated in Seahorse XF DMEM medium (Agilent Technologies, USA) supplemented with 10 mM glucose, 1 mM pyruvate, and 2 mM glutamine. A FluxPak XFe24 sensor cartridge was loaded with 1 μM oligomycin, 0.5 μM FCCP (Carbonyl cyanide 4-(trifluoromethoxy)phenylhydrazone), and 0.5 μM rotenone/antimycin A (RO/AA) from the Seahorse XF Mito-stress test kit (Agilent Technologies, USA). Data were analyzed using Wave Desktop Software 2.6 (Agilent Technologies, USA), and results were exported to Excel using the Report Generator.

Expression of tagged proteins in cardiomyocytes

EGFP-tagged CCDC141 isoforms were expressed in neonatal rat cardiomyocytes using a baculovirus-mediated system, with modifications to established protocols[36,40,43,44]. Briefly, CCDC141 isoforms were PCR-amplified from mouse heart cDNA and cloned into the pFastBac-VSVG-CMV-EGFP-WPRE vector. The resulting plasmids were transformed into *E. coli* DH10Bac for bacmid production, following the manufacturer's instructions (Thermo-Fisher Scientific, USA). Bacmids were transfected into Sf9 insect cells using Cellfectin II reagent (Thermo-Fisher Scientific, USA), and baculoviruses were generated in SF-900 II SFM medium (Thermo-Fisher Scientific, USA). Neonatal rat cardiomyocytes (2 days old) were isolated using the Neonatal Heart Dissociation Kit (Miltenyi Biotec, Germany) and gentleMACS Octo Dissociator with Heaters (Miltenyi Biotec), following the kit protocol. After a 2-h pre-plating step to remove non-cardiomyocytes, cardiomyocytes were cultured on laminin-coated vessels in DMEM supplemented with 10% FBS, penicillin/streptomycin, and cytosine arabinoside (Ara-C) at 37 °C in 5% CO_2 for 2 days. Cardiomyocytes were then infected with baculovirus in serum-free MEM medium for 4 h, followed by treatment with BacMam enhancer (Invitrogen, USA) in DMEM for 1 h. The medium was subsequently replaced with DMEM containing 10% FBS, and cardiomyocytes were cultured for an additional day. Cardiomyocytes were fixed in paraformaldehyde at 37 °C for 15 min, washed with PBS, permeabilized with 0.1% Triton-X-100 for 5 min, and blocked with BlockOne (1:20 in PBS; Nakalai Tesque, Japan) for 1 h. Cardiomyocytes were then stained with anti-GFP (Abcam, ab290) and anti-α-actinin (Sigma, A7811) antibodies, followed by Alexa Fluor 488- or 568-conjugated secondary antibodies (Thermo-Fisher Scientific, USA) for 1 h. Nuclei were counterstained with DAPI for 10 min and mounted in fluorescence mounting medium (DAKO, Denmark). Imaging was performed using a Zeiss LSM 900 confocal microscope equipped with Airyscan 2 (Zeiss, Germany). Fluorescence intensity linescan plots were visualized using the Plot profile tool in ImageJ 1.54p software (NIH, USA).

RNA preparation, PCR, and real-time PCR

Tissues were stabilized with RNAlater® Stabilization Reagent (QIAGEN, Germany) and homogenized with a Polytron™ homogenizer (PT1600E; Kinematica, Switzerland). Cultured cardiomyocytes were harvested without homogenization. Total RNA was extracted using ISOGEN or ISOGEN-II system (Nippon Gene, Japan), and RNA yield and quality were assessed using a NanoDrop spectrophotometer (ND-1000; Thermo-Fisher Scientific, USA). The cDNAs were synthesized using PrimeScript-II Reverse Transcriptase (Takara Bio, Japan) with random primers or PrimeScript RT Master Mix (Takara Bio, Japan). The cDNAs for specific proteins were PCR-amplified using Phusion polymerase (New England Biolabs, USA), purified with a GEL/PCR Purification Mini Kit (Favorgen, Taiwan), and cloned into appropriate vectors. Quantitative real-time PCR (qPCR) was performed using SYBR® Green Real-Time PCR Master Mixes (Thermo-Fisher Scientific, USA) on a StepOnePlus™ real-time PCR system (Thermo-Fisher Scientific, USA). The specific primers are listed in Supplementary Table 1. Relative mRNA expression levels were quantified using the ΔΔCT method, with 18S rRNA or GAPDH as reference genes. For pathway-level analysis, the PrimerArray® Mouse Focal adhesion panel (Takara Bio, Japan) was used to assess gene expression related to focal adhesion pathway.

RNA-Seq

RNA-Seq analysis was performed as previously described[36]. Briefly, total RNA yield and quality were assessed using the 2100 Bioanalyzer (Agilent Technologies, USA). RNA-seq libraries were prepared using TruSeq Stranded mRNA Library Prep Kit (Illumina, USA), and the quality was evaluated with 2200 TapeStation (Agilent Technologies, USA). Paired-end sequencing was conducted on an Illumina HiSeq 2500 platform (Hokkaido System Science, Japan). The obtained data were processed using the following programs. Known adapters and low-quality reads were trimmed using Cutadapt 1.1 and Trimmomatic 0.32, respectively. Cleaned reads were mapped to the mouse reference genome (GRCm38, Release 92) using Tophat 2.0.14. The normalized expression values for each transcript were quantified as fragments per kilobase of exon model per million mapped fragments (FPKM) using Cufflinks 2.2.1. Gene ontology (GO) and KEGG

pathway enrichment analyses were performed using DAVID 6.8. RNA-Seq data from one wild-type and one knockout mouse were analyzed. Differentially expressed genes were defined as upregulated (>2-fold) or downregulated (< 0.5-fold) in the KO mouse compared to the wild-type. A total of 477 differentially expressed genes were identified. RNA-Seq data have been deposited in the DDBJ Sequence Read Archive under accession number DRR442927. For comparison, simultaneously sequenced RNA-seq data from a wild-type mouse (DDBJ/EMBL/GenBank accession DRR215904)[36] were reprocessed using the same pipeline.

Yeast two-hybrid screening

Protein-protein interactions were screened using Matchmaker™ Two-Hybrid System 3 or Matchmaker™ Gold Yeast Two-Hybrid System (Takara Bio, Japan). Briefly, connectin C-zone super-repeat 1, P-zone Ig-Fn3-Kinase, and CCDC141 were cloned into pGBKT7 bait vector and transformed into yeast strains AH109 or Y2HGold. The transformants were mated with yeast strain Y187 containing prey cDNA libraries derived from human heart tissue (Mate & Plate™ Library; Takara Bio, Japan) or normalized universal human tissues (Normalized Mate & Plate™ Library; Takara Bio, Japan). Mated yeasts were selected on synthetic dropout (SD) medium lacking tryptophan, leucine, and histidine (for AH109) or tryptophan, leucine, histidine, and alanine (for Y2HGold). Positive interactions were confirmed using β-galactosidase (AH109) or α-galactosidase (Y2HGold) assays. Prey plasmids from positive clones were isolated and sequenced to identify candidate binding partners. To determine binding domains, truncated CCDC141 constructs in pGBKT7 and the identified nesprin-1 prey clones were separately transformed into Y2HGold and Y187 strains, respectively. Mated yeast cells were plated on SD medium lacking tryptophan, leucine, histidine, and adenine, and screened using α-galactosidase activity.

Pull-down experiments

For pull-down assays, the N- and C-terminal region of CCDC141 was cloned into pGEX6P-1 vector, the C-terminal region of nesprin-1 and connectin P-zone FN3-Kin were cloned into pRSET-A vector, and connectin C-zone SR1 was cloned into pETM44 vector. The resulting glutathione S-transferase (GST)-, 6×His- or maltose binding protein (MBP)-tagged constructs were expressed in *E. coli* SoluBL21 (Genlantis, USA) and purified using glutathione sepharose 4B (GE Healthcare, USA), Ni-NTA affinity chromatography (Qiagen, Germany), or MBP affinity columns, respectively. Purified proteins were stored at −80 °C in 25% glycerol until use. β-Connectin (titin-II) was prepared from rabbit back muscle as previously described[45]. For binding assays, GST-tagged proteins were immobilized on 20 µL of glutathione sepharose 4B beads. His-tagged or MBP-tagged proteins were incubated with the beads in 200 µL of pull-down buffer (80 mM KCl, 2 mM $MgCl_2$, 10 mM HEPES, 1 mM DTT, 1% Triton-X, pH 7.3) for 30 min at room temperature with tapping every 5 min. Beads were washed five times with 200 µL of pull-down buffer and eluted with SDS sample buffer. Eluted proteins were separated by SDS-PAGE, transferred to nitrocellulose membranes, and detected by Western blot.

SDS-PAGE, Western blot, and SDS-Vertical agarose gel electrophoresis

Tissues were homogenized using a Polytron™ homogenizer (PT1600E; Kinematica, Switzerland) in a sample buffer containing 8 M urea, 2 M thiourea, 3% SDS, 75 mM DTT, 0.03% bromophenol blue, and 0.05 M Tris-HCl (pH 6.8), supplemented with Halt™ protease inhibitor cocktail (Thermo-Fisher Scientific, USA). Samples were heated at 60 °C for 10 min and centrifuged. Proteins in the supernatant were separated by SDS-PAGE, transferred onto a nitrocellulose membrane, blocked with 5% skim milk or 5% BSA, and probed with primary and secondary antibodies. Horseradish peroxidase (HRP)-conjugated IgG was visualized using enhanced chemiluminescence (Western Lightning ECL-Pro; PerkinElmer, USA) and imaged with either a LAS4000mini luminescent image analyzer (GE Healthcare, USA) or an Amersham Imager 680 (GE Healthcare, USA). Alkaline phosphatase (AP)-conjugated IgG was visualized using a chromogenic substrate nitroblue tetrazolium (NBT)/5-bromo-4-chloro-3-indolyl phosphate (BCIP). For connectin analysis, supernatants were electrophoresed on 1% vertical agarose gels containing 30% glycerol, 0.05 M Tris base, 0.384 M glycine, and 0.1% SDS at 10 mA for ~2 h[46]. The lower electrophoresis buffer consisted of 0.05 M Tris base, 0.384 M glycine, and 0.1% SDS, while the upper buffer contained the same components plus 10 mM β-mercaptoethanol. Proteins were visualized using Coomassie brilliant blue (Bio-Safe CBB G-250; Bio-Rad, USA).

Antibodies

Rabbit polyclonal antibodies against CCDC141 were generated using either the rat CCDC141 N-terminal region (XP_003749542.2; amino acids 1–466) or a synthetic peptide corresponding to mouse CCDC141 (NP_001020747.2; amino acids 1276–1291; sequence: CDGGHSKKDTFTSHFER). Antibodies against other proteins were obtained as follows: Connectin C-term (Pc72C[47]), MBP-tag (custom made), 6xHis-tag (Abcam, ab49746), GFP (Abcam, ab290), α-Actinin (Sigma, A7811), Vinculin (Sigma, V9131), Filamin-C (Invitrogen, PA5-88919), Nesprin-1 (ImmuQuest, IQ568), Phospho-PDK1 (CST, 3438), Phospho-PTEN (CST, 9551), Phospho-c-Raf (CST, 9421), Akt (CST, 4691), Phospho-Akt (CST, 4060), mTOR (CST, 2983), Phospho-mTOR (CST, 5536), Phospho-GSK-3β (CST, 5558), Phospho-Myosin Light Chain 2 (CST, 3671), RyR2 (Invitrogen, MA3-916), SERCA2a (Invitrogen, MA3-919), NCX1 (Abcam, ab2869), PLN (CST, 8495), p-PLN (CST, 8496), COXIV (CST, 4844), MFN2 (Proteintech, 12186-1-AP), ACTB (Santa Cruz, sc-81178), and GAPDH (Santa Cruz, sc-32233). Antibody dilutions are listed in Supplementary Tables 2 and 3.

Statistics and reproducibility

All data are presented as means ± standard error of the mean (SEM). Statistical comparisons between two groups were performed using a two-tailed unpaired Student's t-test in Microsoft Excel (versions 2016 and 2024). A p-value < 0.05 was considered statistically significant. Significance levels were denoted as follows: n.s., not significant; $*p < 0.05$; $**p < 0.01$; $***p < 0.001$. No statistical tests were used to predetermine the sample sizes. Additional statistical details, including sample sizes and p-values for individual experiments, are provided in figure legends.

Reporting summary

Further information on research design is available in the Nature Portfolio Reporting Summary linked to this article.

Data availability

All data pertaining to this work are shown in the text, figures, and supplementary information. Supplementary Information contains supplementary Figs. 1–6, primer sequences used for qPCR experiments (Supplementary Tables 1), antibody information used for western blot and immunofluorescence microscopy (Supplementary Tables 2 fand 3), and uncropped images of blots. Supplementary Data are values for all data points shown in the graphs and charts. Raw RNA-seq data of wild-type and CCDC141-KO ventricles are available in the DDBJ/EMBL/GenBank sequencing read archive under the accession numbers DRR442927 and DRR215904.

Received: 22 October 2024; Accepted: 18 October 2025;
Published online: 26 November 2025

References

1. Lyon, R. C., Zanella, F., Omens, J. H. & Sheikh, F. Mechanotransduction in cardiac hypertrophy and failure. *Circ. Res* **116**, 1462–1476 (2015).
2. Granzier, H. L. & Labeit, S. Discovery of titin and its role in heart function and disease. *Circ. Res* **136**, 135–157 (2025).

3. Loescher, C. M., Hobbach, A. J. & Linke, W. A. Titin (TTN): from molecule to modifications, mechanics, and medical significance. *Cardiovasc. Res.* **118**, 2903–2918 (2022).
4. van der Pijl, R. J. et al. The titin N2B and N2A regions: biomechanical and metabolic signaling hubs in cross-striated muscles. *Biophys. Rev.* **13**, 653–677 (2021).
5. Bogomolovas, J. et al. Titin kinase ubiquitination aligns autophagy receptors with mechanical signals in the sarcomere. *EMBO Rep*. **22**. https://doi.org/10.15252/embr.201948018 (2021).
6. Lombardi, M. L. et al. The interaction between Nesprins and sun proteins at the nuclear envelope is critical for force transmission between the nucleus and cytoskeleton. *J. Biol. Chem.* **286**, 26743–26753 (2011).
7. Banerjee, I. et al. Targeted ablation of Nesprin 1 and Nesprin 2 from murine myocardium results in cardiomyopathy, altered nuclear morphology and inhibition of the biomechanical gene response. *PLoS Genet.* **10**, e1004114 (2014).
8. Puckelwartz, M. J. et al. Nesprin-1 mutations in human and murine cardiomyopathy. *J. Mol. Cell. Cardiol.* **48**, 600–608 (2010).
9. Waardenberg, A. J. et al. Phosphoinositide 3-kinase (PI3K(p110α)) directly regulates key components of the Z-disc and cardiac structure. *J. Biol. Chem.* **286**, 30837–30846 (2011).
10. Labeit, S. et al. Expression of distinct classes of titin isoforms in striated and smooth muscles by alternative splicing, and their conserved interaction with filamins. *J. Mol. Biol.* **362**, 664–681 (2006).
11. Eijgelsheim, M. et al. Genome-wide association analysis identifies multiple loci related to resting heart rate. *Hum. Mol. Genet.* **19**, 3885–3894 (2010).
12. Arking, D. E. et al. Genetic association study of QT interval highlights role for calcium signaling pathways in myocardial repolarization. *Nat. Genet*. **46**, 826–836 (2014).
13. Sotoodehnia, N. et al. Common variants in 22 loci are associated with QRS duration and cardiac ventricular conduction. *Nat. Genet*. **42**, 1068–1076 (2010).
14. Norland, K. et al. Sequence variants with large effects on cardiac electrophysiology and disease. *Nat. Commun.* **10**, 4803 (2019).
15. Hoffmann, T. J. et al. Genome-wide association analyses using electronic health records identify new loci influencing blood pressure variation. *Nat. Genet.* **49**, 54–64 (2017).
16. Warren, H. R. et al. Genome-wide association analysis identifies novel blood pressure loci and offers biological insights into cardiovascular risk. *Nat. Genet*. **49**, 403–415 (2017).
17. Wang, Q. et al. Epistasis regulates genetic control of cardiac hypertrophy. *Nat. Cardiovasc. Res.* **4**, 740–760 (2025).
18. Weng, L. C. et al. Meta-analysis of genome-wide association studies reveals genetic mechanisms of supraventricular arrhythmias. *Circ. Genom. Precis. Med.* **17**, e004320 (2024).
19. Weng, L. C. et al. The impact of common and rare genetic variants on bradyarrhythmia development. *Nat. Genet*. **57**, 53–64 (2025).
20. Fukuda, T., Sugita, S., Inatome, R. & Yanagi, S. CAMDI, a novel disrupted in schizophrenia 1 (DISC1)-binding protein, is required for radial migration. *J. Biol. Chem.* **285**, 40554–40561 (2010).
21. Tsukamoto, O. & Kitakaze, M. Biochemical and physiological regulation of cardiac myocyte contraction by cardiac-specific myosin light chain kinase. *Circ. J.* **77**, 2218–2225 (2013).
22. Centner, T. et al. Identification of muscle specific ring finger proteins as potential regulators of the titin kinase domain. *J. Mol. Biol.* **306**, 717–726 (2001).
23. Witt, C. C. et al. Cooperative control of striated muscle mass and metabolism by MuRF1 and MuRF2. *EMBO J.* **27**, 350–360 (2008).
24. Wei, L. et al. Integrin β3 promotes cardiomyocyte proliferation and attenuates hypoxia-induced apoptosis via regulating the PTEN/Akt/mTOR and ERK1/2 pathways. *Int. J. Biol. Sci.* **16**, 644–654 (2020).
25. Suryakumar, G., Kasiganesan, H., Balasubramanian, S. & Kuppuswamy, D. Lack of β3 integrin signaling contributes to calpain-mediated myocardial cell loss in pressure-overloaded myocardium. *J. Cardiovasc. Pharmacol.* **55**, 567–573 (2010).
26. Fukuda, T. et al. Rescue of CAMDI deletion-induced delayed radial migration and psychiatric behaviors by HDAC 6 inhibitor. *EMBO Rep.* **17**, 1785–1798 (2016).
27. Miragoli, M. et al. Microtubule-dependent mitochondria alignment regulates calcium release in response to nanomechanical stimulus in heart myocytes. *Cell Rep.* **14**, 140–151 (2016).
28. Pasqualini, F. S., Nesmith, A. P., Horton, R. E., Sheehy, S. P. & Parker, K. K. Mechanotransduction and metabolism in cardiomyocyte microdomains. *BioMed. Res. Int.* **2016**, 1–17 (2016).
29. Goto, Y., Slinker, B. K. & LeWinter, M. M. Decreased contractile efficiency and increased nonmechanical energy cost in hyperthyroid rabbit heart. Relation between O2 consumption and systolic pressure-volume area or force-time integral. *Circ. Res* **66**, 999–1011 (1990). Apr.
30. Hata, K. et al. Hypercapnic acidosis increases oxygen cost of contractility in the dog left ventricle. *Am. J. Physiol.* **266**, H730–H740 (1994). Feb.
31. Burkart, C. et al. Modular proteins from the drosophila sallimus (sls) gene and their expression in muscles with different extensibility. *J. Mol. Biol.* **367**, 953–969 (2007).
32. Katzemich, A. et al. The function of the M-line protein, obscurin, in controlling the symmetry of the sarcomere in Drosophila flight muscle. *J.Cell Sci.* jcs.097345. https://doi.org/10.1242/jcs.097345 (2012).
33. Hanashima, A., Usui, Y., Hashimoto, K. & Mohri, S. The ancestor and evolution of the giant muscle protein connectin/titin. *J. Mol. Evol.* **93**, 306–321 (2025).
34. Greer, C. et al. Deleterious variants in genes regulating mammalian reproduction in Neanderthals, Denisovans and extant humans. *Hum. Reprod.* **36**, 734–755 (2021).
35. Ujihara, Y. et al. Induced NCX1 overexpression attenuates pressure overload-induced pathological cardiac remodelling. *Cardiovasc Res.* **111**, 348–361 (2016).
36. Hashimoto, K. et al. Postnatal expression of cell cycle promoter Fam64a causes heart dysfunction by inhibiting cardiomyocyte differentiation through repression of Klf15. *iScience* **25**, 104337 (2022).
37. Hoshino, M. et al. Optical properties of in situ eye lenses measured with X-ray Talbot interferometry: a novel measure of growth processes. *PLoS ONE* **6**, e25140 (2011).
38. Hu, Y., Limaye, A. & Lu, J. Three-dimensional segmentation of computed tomography data using Drishti Paint: new tools and developments. *R. Soc. Open Sci.* **7**, 201033 (2020).
39. Hanashima, A. et al. Complete primary structure of the I-band region of connectin at which mechanical property is modulated in zebrafish heart and skeletal muscle. *Gene* **596**, 19–26 (2017).
40. Hashimoto, K. et al. Fam64a is a novel cell cycle promoter of hypoxic fetal cardiomyocytes in mice. *Sci. Rep.* **7**, 4486 (2017).
41. Ujihara, Y. et al. Elimination of fukutin reveals cellular and molecular pathomechanisms in muscular dystrophy-associated heart failure. *Nat. Commun.* **10**, 5754 (2019).
42. Ackers-Johnson, M. et al. A simplified, langendorff-free method for concomitant isolation of viable cardiac myocytes and nonmyocytes from the adult mouse heart. *Circ. Res* **119**, 909–920 (2016).
43. Hashimoto, K. et al. Nuclear connectin novex-3 promotes proliferation of hypoxic foetal cardiomyocytes. *Sci. Rep.* **8**, 12337 (2018).
44. Hashimoto, K. et al. Loss of connectin novex-3 leads to heart dysfunction associated with impaired cardiomyocyte proliferation and abnormal nuclear mechanics. *Sci. Rep.* **14**, 13727 (2024).
45. Kimura, S. et al. Characterization and localization of α-connectin (titin 1): An elastic protein isolated from rabbit skeletal muscle. *J. Muscle Res. Cell Motil.* **13**, 39–47 (1992).

46. Warren, C. M., Krzesinski, P. R. & Greaser, M. L. Vertical agarose gel electrophoresis and electroblotting of high-molecular-weight proteins. *Electrophoresis* **24**, 1695–1702 (2003).
47. Soeno, Y. et al. Organization of connectin/titin filaments in sarcomeres of differentiating chicken skeletal muscle cells. *Mol. Cell. Biochem.* **190**, 125–131 (1999).
48. Hanashima, A. Obituary: Sumiko Kimura 1947–2018. *J. Muscle Res. Cell Motil.* **39**, 149–151 (2018).
49. Hanashima, A., Kawamura, Y. & Nakauchi, Y. A great legacy of muscle research and education from Dr. Sumiko Kimura. *Cytoskeleton* **76**, 298–302 (2019).

Acknowledgements

We sincerely appreciate Dr. Moldir Myrzabekova of the Medical Faculty Mannheim for her invaluable assistance with the yeast two-hybrid infrastructure. We thank Mr. N. Iwachido and Mr. N. Matsuda at Kawasaki Medical School for their technical support with histological and EM experiments. We also thank Dr. A. Gasch in the Medical Faculty Mannheim for the antibody production. This paper is in memory of Dr. Sumiko Kimura[48,49] and Dr. Dittmar Labeit, our co-authors, who pioneered this, as many other studies, and passed away in 2018 and 2019, respectively. This work was supported by JSPS KAKENHI Grant Numbers 16K01385, 20H04508, and 24K03254 to A.H., 23H03855 to Yo.U., 24K03270 to K.H., and 23H00556 to S.M. This work is also supported by Research Grants from the Kawasaki Medical School, Okayama Medical Foundation, Sanyo Broadcasting Foundation, and Ryoubi Teien Memory Foundation to A.H.

Author contributions

A.H., Y.o.U., K.H., S.L., and S.M. designed the experiments; A.H., M.K., Y.o.U., K.H., S.W., and S.M. performed the experiments; A.H., Y.o.U., K.H., T.M., S.L., and S.M. analyzed the data; A.H., D.L., T.S., and S.K. contributed to antibody production; A.H., M.K., Y.u.U., and M.O. created the animal models; A.H., Y.u.U., K.H., M.H., K.U., and S.M. acquired CT images using a synchrotron; and A.H., S.L., and S.M. wrote the paper.

Competing interests

The authors declare no competing interests.

Additional information

Supplementary information The online version contains supplementary material available at https://doi.org/10.1038/s42003-025-09093-6.

Correspondence and requests for materials should be addressed to Akira Hanashima.

Peer review information *Communications Biology* thanks Thomas G. Martin and the other anonymous reviewers for their contribution to the peer review of this work. Primary handling editor: Dario Ummarino. A peer review file is available.